Investigation and Reduction of EMI Noise Due to the Reverse Recovery Currents of 50/60 Hz Diode Rectifiers

Zhedong Ma, *Student Member, IEEE*, Yiming Li, Shuo Wang, *Fellow, IEEE*, Honggang Sheng, and Srikanth Lakshmikanthan

***Abstract*—Alternating current (ac)/ Direct current (dc) power converters with dc-bus filters can achieve high power density, however, it was found in this article that the reverse recovery currents of the 50/60 Hz diode bridge can lead to significant electromagnetic interference (EMI) noise violating EMI standards above 150 kHz. This article analyzed and quantified the mechanism of the EMI generation due to the reverse recovery currents of the 50/60 Hz diodes. It was found that although the reverse recovery of the 50/60 Hz diode bridge repeats at a frequency of 50/60 Hz, the EMI can be very high above 150 kHz due to the operating principle of electromagnetic compatibility spectrum analyzers. Two techniques were proposed to reduce the EMI due to the reverse recovery of the diode bridge. The analyses were validated by either simulations or experiments.**

***Index Terms*—AC/DC power adapter, diode bridge, electromagnetic interference (EMI), reverse recovery current.**

I. Introduction

ELECTROMAGNETIC interference (EMI) is a very important issue in power electronics applications, especially in high frequency (HF) ac/dc power conversion applications. The ac/dc power converters, such as flyback converters in Fig. 1(a), usually employ a diode bridge between the converter and an ac source to rectify ac to dc. To reduce differential mode (DM) EMI, the dc bus filter composed of C_{DC}, L_{DM}, and C_2 in Fig. 1(a) is designed to meet the EMI standard [1], [2]. Based on the research in [1] and [2], the dc-bus filter with split bulk capacitors (C_{DC} and C_2) can achieve a much smaller size than the ac line DM filter since dc capacitors instead of ac capacitors can be used and the current ripple in a dc-bus inductor is much smaller than that

Manuscript received November 7, 2021; revised February 10, 2022, April 12, 2022, and May 20, 2022; accepted May 23, 2022. Date of publication June 3, 2022; date of current version July 13, 2022. This work was supported by Google Inc. *(Corresponding author: Shuo Wang.)*

Zhedong Ma and Yiming Li are with the University of Florida, Gainesville, FL 32611 USA (e-mail: zhedongma@ufl.edu; brighturan@ufl.edu).

Shuo Wang is with the Department of Electrical and Computer Engineering, University of Florida, Gainesville, FL 32611 USA (e-mail: shuowang@ieee.org).

Honggang Sheng and Srikanth Lakshmikanthan are with the Google Inc., Mountain View, CA 94043 USA (e-mail: honggangs@google.com; srikanthl@google.com).

Color versions of one or more figures in this article are available at https://doi.org/10.1109/JESTIE.2022.3179985.

Digital Object Identifier 10.1109/JESTIE.2022.3179985

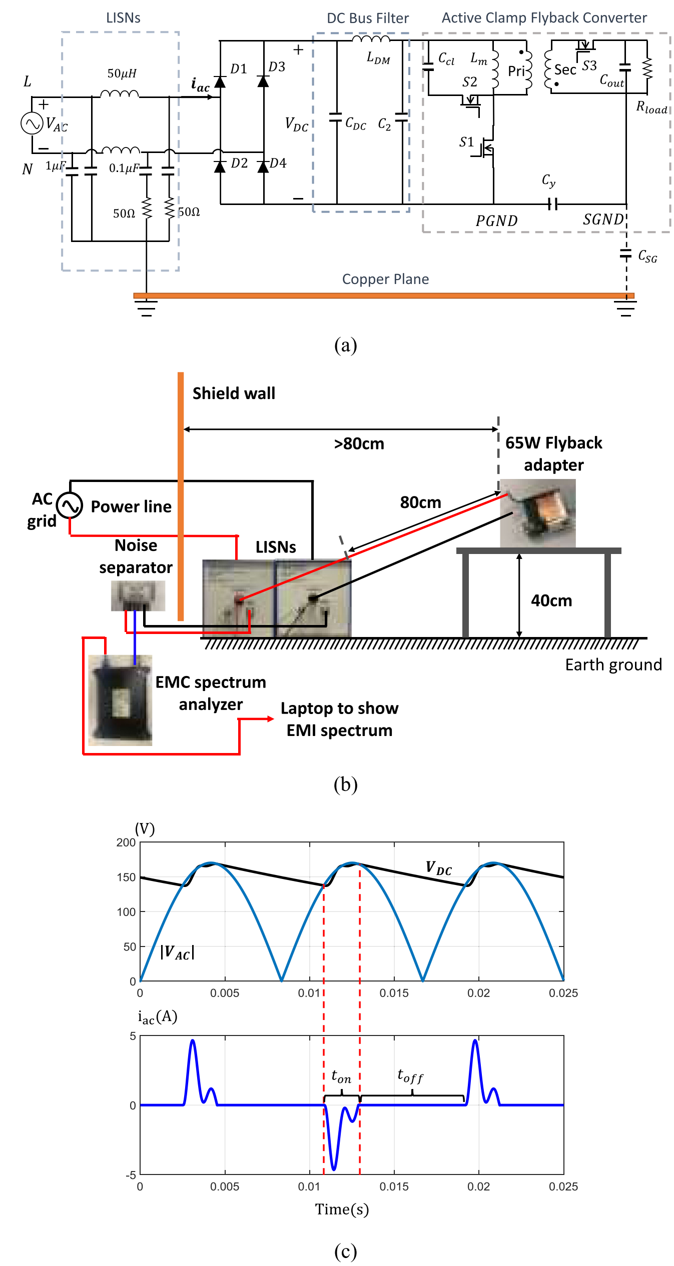

Fig. 1. (a) Flyback converter under investigation with LISNs. (b) Setup for measurement. (c) Voltage and current waveforms of the diode bridge rectifier.

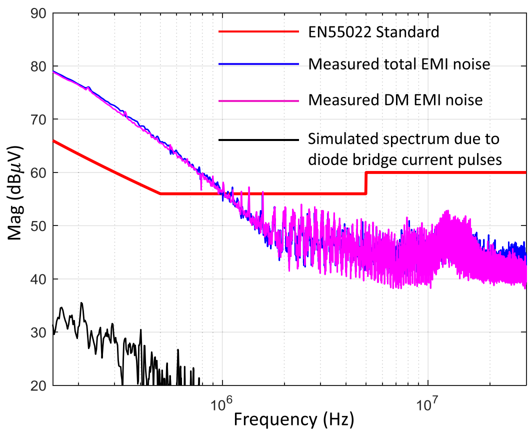

Fig. 2. Comparison of the measured and simulated EMI spectra.

in an ac line inductor. Because of this, some HF and high-power density power converters employ dc bus filters after the diode bridge. In Fig. 1(a), two line-impedance stabilization networks (LISNs) are inserted between the power source and the converter for EMI measurement. Fig. 1(b) shows the measurement setup and the prototype under investigation. The diode rectifier turns ON when the ac voltage V_{AC} is higher than the dc-bus voltage V_{DC} and turn OFF when the bridge input ac voltage is lower than V_{DC}. As a result, the current i_{ac} only flows through the diode bridge within part of the half ac-line period, generating current pulses on the ac input as shown in Fig. 1(c). The bumps in i_{ac} are due to the resonance of grid impedance, LISN's inductance and the dc bus capacitors. The current pulses have a fundamental frequency of 50/60 Hz. The magnitudes of the current harmonics reduce quickly as frequency increases. The conductive EMI standards such as EN55022 has a frequency range from 150 kHz to 30 MHz, which is much higher than 50/60 Hz, so these harmonics are not supposed to generate high EMI noise within 150 kHz–30 MHz.

In Fig. 1(a), the switching frequency of the converter is 105 kHz with an output power of 65 W. The input is 120 V ac at 60 Hz and the output voltage is 20 V dc.

The total conductive EMI was measured from the 50Ω load resistance in one of the LISNs based on the setup defined in EN55022 class B as shown in Fig. 1(a) and (b). The resolution bandwidth (RBW) of the spectrum analyzer Tektronix RSA306B used in the measurement was 9 kHz as required by the standard. The spectrum analyzer was set to maximum hold mode to measure the worst EMI.

The measured total peak EMI on one LISN is shown in Fig. 2. The EMI on the other LISN is almost the same as that in Fig. 2 so it is not shown here. The DM EMI was also measured using a noise separator [3] in Fig. 2. It is shown that the measured total EMI is much higher than the EMI standard and it is dominated by the DM EMI. The simulated EMI spectrum due to the current pulses generated by the diode bridge is also shown in Fig. 2. Because it is much smaller than the measured DM EMI, the measured high DM EMI is not caused by these current pulses. It was also found that the measured DM EMI below 1 MHz is almost unchanged no matter how good the dc-bus filter is designed.

Because of this, the high DM EMI is generated by something else which has not been disclosed at present [4]–[17]. Scheich and Roudet [18] analyzed the contribution of the shoot-through currents of a silicon-controlled rectifier bridge during the extended conducting duration to the EMI. It is concluded in the article that the generated EMI due to the reverse recovery current is insignificant. In [19], the authors investigated the high DM EMI noise caused by the resonance between EMI filters and the diode rectifier, particularly with a weak grid. However, the reverse recovery currents of the diode rectifier were not discussed. Makaran [20] investigated the impact of SiC diodes on EMI, however, it concluded that it is the switching transient, not the reverse recovery currents, that leads to the high EMI. The effect of the reverse-recovery currents of SiC diodes versus Si diodes was studied in [21], however, it concluded that the abrupt cut off reverse recovery currents do not contribute to the high EMI noise below 10 MHz significantly. The work in [22]–[24] focus on the EMI due to the reverse recovery of fast switching diodes antiparalleled with the switching devices instead of the EMI due to the reverse recovery currents of low frequency diode rectifiers. Different from these papers, for the first time, this article discloses how the reverse recovery currents of a slow diode bridge of an ac/dc converter can generate significant EMI at low frequencies, which has never been disclosed in any literatures

In this article, it was found that the measured high different mode (DM) EMI below 1 MHz of an ac/dc converter could be due to the reverse recovery currents of the 50/60 Hz diode rectifier, instead of the switching current of the power converter. After an extensive researching of existing literatures, it was found that this issue has not been studied. Because the dc bus DM filters are used in many designs because of its advantages mentioned previously, this article will analyze the mechanism of high DM EMI generated by the low-speed diode bridge. The contribution of this article includes as follows.

1) The mechanism of high DM EMI due to the reverse recovery current of a slow diode bridge.
2) An EMI model due to the mechanism identified above was developed, quantified, and experimentally verified.
3) Two technical solutions were proposed to reduce the DM EMI due to the slow diode bridge.
4) Cost and size were analyzed for the proposed two solutions."

The rest of the article was organized as follows. in Section II, the reverse recovery currents of the diode rectifier were identified as a major EMI source and the mechanism of generating high EMI was analyzed in time domain. In Section III, simulations and experiments were conducted to verify the analysis in frequency domain. In Section IV, two techniques were proposed to reduce the EMI noise due to the diode reverse recovery currents. Both techniques were verified with experiments. Finally, Section V concludes this article.

II. Investigating How EMI is Generated

A. Identify the Diode Rectifier as a Major Noise Source

Fig. 3 shows the measurement setup used for identifying the EMI noise source. The system parameters are given in Table I.

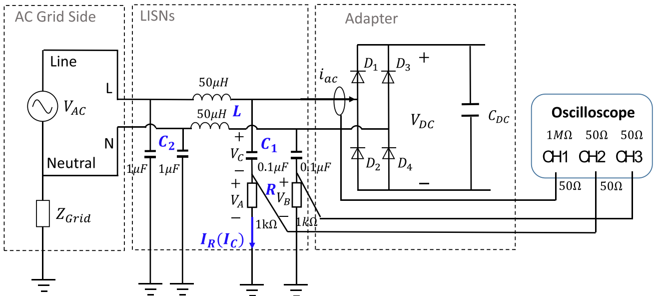

Fig. 3. Measurement setup for i_{ac} and output voltages V_A and V_B of LISNs.

TABLE I
System Parameters

Parameters	Value	Parameters	Value
V_{AC} (AC excitation)	120V/60Hz	LISN's L	$50\mu H$
Capacitor C_{DC}	$82\mu F$	LISN's resistance	1k Ω /50Ω
Output power	65W	LISN's C1	$0.1\mu F$
Diode for rectifier	SD560BTR	LISN's C2	$1\mu F$

In the measurement, in order to validate the high EMI below 1MHz is caused by the diode bridge instead of the flyback converter, the measurements were conducted for two cases: a 65 W flyback converter is connected to the dc bus, and a 65 W resistor load (350 Ω) is connected to the dc bus. The oscilloscope is RIGOL MSO4054 with 500 MHz bandwidth. The channels 2 and 3 are used to measure EMI noise voltage drops V_A and V_B on two LISNs. The input impedances of channels 2 and 3 are set to 50 Ω to meet the LISNs' load resistance requirement. The channel 1 is used to measure input ac current i_{ac}. The input impedance of channel 1 is set to 1 MΩ for current measurement. The current probe is Yokogawa 701932 with a bandwidth of 100 MHz.

Fig. 4 shows the measured results with the flyback converter and the load resistor. In Fig. 4(a), for V_A, during t_0-t_1, the 60 Hz leakage current flowing through 0.1 μF capacitor and 50 Ω in LISNs is dominant. For V_B, it is out of phase from V_A. i_{ac} is zero since the diode bridge is OFF. At t_1, the magnitude of V_{AC} begins to be larger than dc-bus voltage V_{DC}, the diode bridge begins to conduct currents. During the turn-ON transient, di_{ac}/dt abruptly increases from zero to around 4 kA/s at t_1, as a result, a high voltage spike is induced on two LISN's 50 μH inductors. Since the voltages of two 0.1uF LISN capacitors are almost constant during this short duration, a voltage dip is induced on V_A and V_B right after t_1, respectively in Fig. 4(a).

After the diode bridge begins to conduct currents, because the impedance of 1 μF capacitor is much higher than the impedance of 50 μH at low frequencies, the inductance of power grid is in series with the two LISN's 50 μH inductors and they resonate with the 82 μF capacitor on the dc bus after the diode bridge. This results in a 750 Hz resonant current i_{ac} as shown in Fig. 4(a). The voltage across the outputs of two LISNs is equal to the voltage V_{DC} on C_{DC} and its ac components, which include the resonant voltage on C_{DC}, is coupled to the 50 Ω load resistors of LISNs via

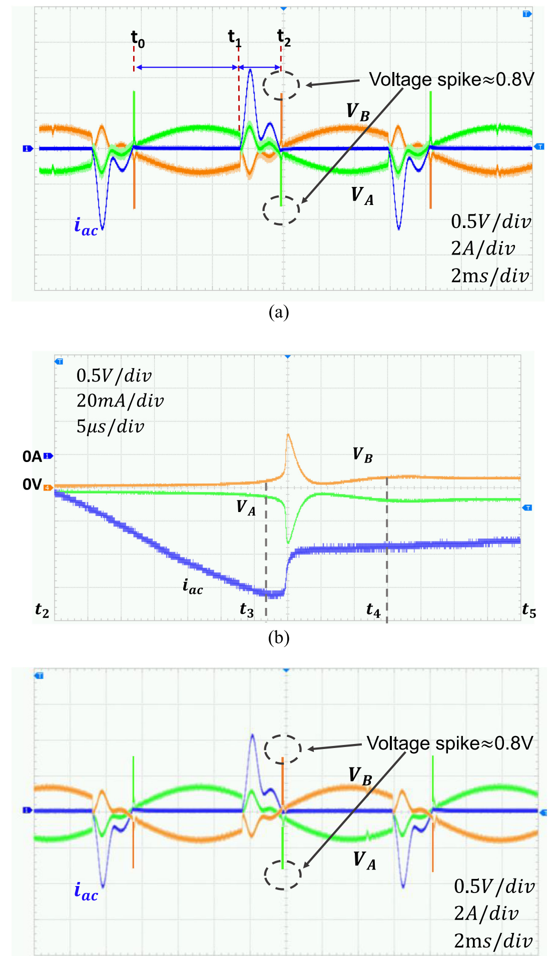

Fig. 4. (a) Measured V_A, V_B, and i_{ac} with a flyback converter load. (b) Zoomed-in picture for the reverse recovery response. (c) Measured V_A, V_B, and i_{ac} with a resistor load.

two 0.1 μF capacitors. In Fig. 3, since the impedance of LISN's 0.1 μF capacitor at 60 Hz is much higher than 50 Ω resistance while LISN's 50 μH inductance is nearly short-circuited at 60 Hz, V_A is 90° leading V_{AC}, which can be explained with (1) and (2). As a result, V_A has the resonant voltage waveforms in phase with i_{ac} as in Fig. 4(a). Similarly, the similar analysis applies to V_B too

$$\dot{I}_R = \dot{I}_C = j\omega C_1 \dot{V}_C \approx \frac{1}{2} j\omega C_1 \dot{V}_{\text{AC}} \tag{1}$$

$$\dot{V}_A = \dot{I}_R \cdot R' \approx \frac{1}{2} j\omega R' C_1 \dot{V}_{\text{AC}}. \tag{2}$$

In (1) and (2), R'= 50Ω //1k Ω , $\dot{I}_R$ and $\dot{I}_C$ are the currents flowing through 50 Ω resistor and 0.1 μF capacitor in LISN's R–C branch. $\dot{V}_A$ and $\dot{V}_C$ represent the voltage drops on 50 Ω resistor and 0.1 μF capacitor, respectively.

At t_2, the input voltage of the bridge begins to be lower than V_{DC}, the diode bridge begins to turn OFF. Since the 60 Hz diode bridge has a long reverse recovery time (>500 ns), a reverse recovery current i_{ac} is observed around t_2 in Fig. 4(a). Fig. 4(b) shows the reverse recovery, which starts from t_2 outside of the

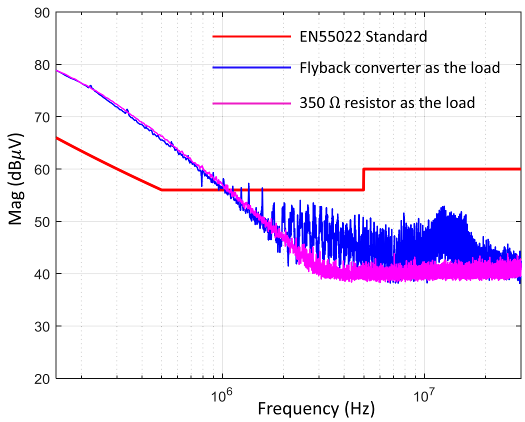

Fig. 5. Comparison of the measured EMI spectra with a resistor load and a flyback converter load.

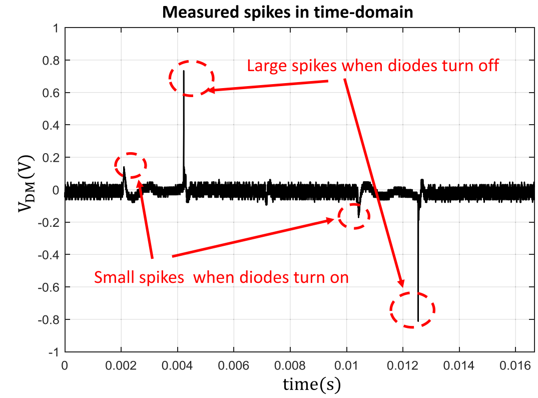

Fig. 6. Measured DM voltage V_{DM} at the output of a DM noise separator.

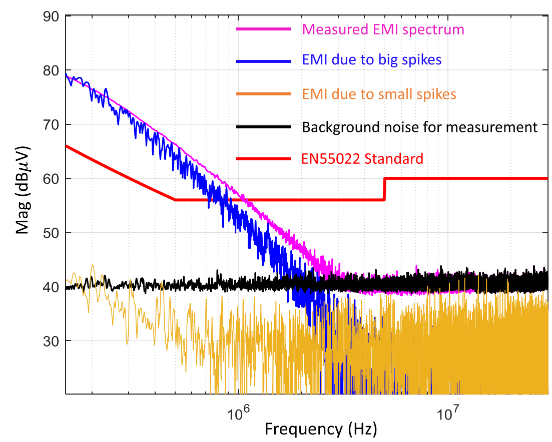

Fig. 7. Comparison of the peak EMI due to two voltage spikes.

figure, and ends at t_5 outside of the figure. Before t_3, the reverse recovery current has a slew rate of -2 kA/s. Starting from t_3, the current slew rate abruptly changes to 16 kA/s. The abrupt current slew rate change during the diode reverse recovery was discussed in the literatures such as [26]. A huge voltage spike is induced on both LISN's 50 μH inductors. As a result, V_A and V_B show huge voltage spikes between t_3 and t_4.

After replacing the flyback converter with a resistor load, the measured voltage and current waveforms in Fig. 4(c) are almost the same as those with the flyback converter. The measured EMI with a resistor load in Fig. 5 is almost the same as that with the flyback converter below 1 MHz. This indicates that the measured voltage spikes in V_A and V_B are from the diode bridge instead of the flyback converter.

Because of this, this article will focus on the detail analysis of the impact of the diode bridge on the measured EMI spectrum and the techniques to reduce the EMI resulted from it.

B. Identify Reverse Recovery Currents as a Major Noise Source

As analyzed in Section II. A, the voltage spikes are induced in V_A and V_B during both turn-ON and turn-OFF transients. It will be explained here that only the voltage spike due to the reverse recovery of the diode bridge during the turn-OFF transient leads to the high EMI noise. Fig. 6 shows the measured DM voltage $V_{\mathrm{DM}} = (V_A\text{-}V_B)/2$ at the output of a DM noise separator [3].

It is shown that the low frequency components, such as that within t_1-t_2, and the 60 Hz leakage current, in i_{ac} have been significantly filtered out by the noise separator because its lower cut off frequency is 10 kHz, as a result, two voltage spikes during reverse recovery transient on V_{DM} are obvious. The voltage spike due to the reverse recovery currents is much higher and narrower than that during the turn-ON transient. V_{DM} can be decomposed to three waveforms: big spikes, small spikes and background noise. As an example, the big spike waveforms can be easily decomposed by using the trace data of the big spikes only and set all the other data to zero. The decomposed big and small spike waveforms were fed to the EMI prediction program developed in [27] to predict the EMI caused by the big or small spikes respectively. The simulated peak EMI spectra are compared in Fig. 7. It should be pointed out that since the noise spike on V_{DM} has a frequency of 60 Hz, the magnitude of the measured EMI using a spectrum analyzer (or the magnitude of the simulated using the program developed based on the operating principle of a spectrum analyzer) with 9 kHz RBW is much higher than that of the FFT result [27]. Using the FFT to predict the measured EMI is thus wrong in this case. This will be explained in Section III.

In Fig. 7, the EMI due to the diode reverse recovery is almost equal to the measured EMI and it is much higher than that during the turn-ON transient. Because of this, the diode reverse recovery currents are identified as the major EMI source.

C. Quantified Analysis

The circuit model used for a quantified analysis is shown in Fig. 8(a). In Fig. 8(a), a pair of diodes ($D1$, $D4$) conduct currents in the firts half line cycle before the reverse recovery happens. The L_{LISN}, C_{LISN}, and R_{LISN} represent the parameters of the LISNs for DM currents. Their impedances are twice of those in a single LISN. It should be pointed out that the grid inductance is not in the circuit because, for the HF harmonics of the reverse recovery currents, the two 1 μF capacitors in LISNs in Fig. 3

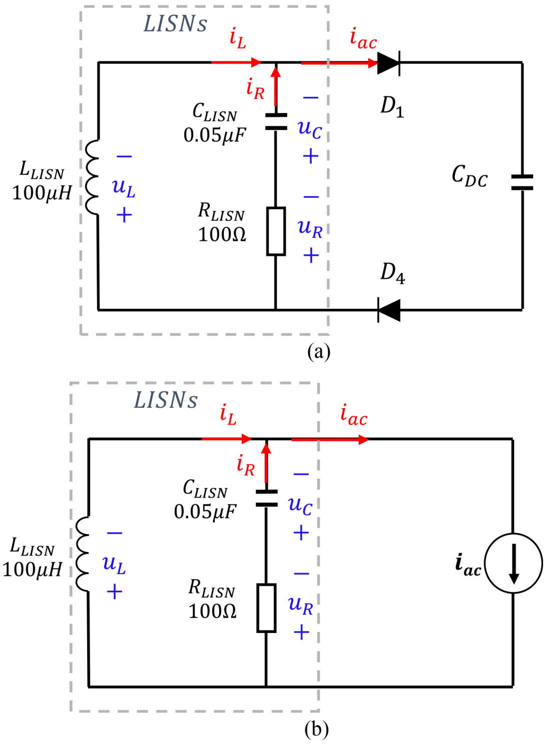

Fig. 8. (a) Circuit model to analyze the impact of the diode reverse recovery currents on the measured EMI.(b) Replacing diodes and C_{DC} with a current source i_{ac}.

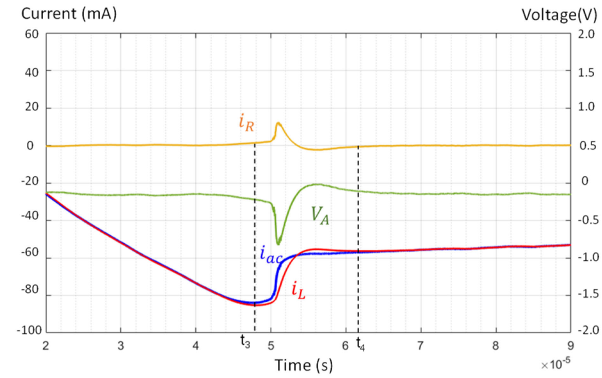

Fig. 9. Simulated currents and V_A during the reverse recovery transient.

have a very small impedance so they isolated grid inductance from the model.

During the short reverse recovery duration, the voltage on C_{DC} is almost constant so it does not influence the reverse recovery. In Fig. 8(b), the diodes and C_{DC} are replaced with a current source i_{ac} which has the exact same current waveform as the original diode current waveform measured with a 100 MHz current probe. Based on the substitution theory, the current i_L flowing through L_{LISN} and i_R flowing through R_{LISN} will be the same as before the diodes were replaced with the i_{ac}. u_R is the voltage drop of i_R on LISNs' two series 50 Ω load resistances.

In Fig. 8, if the voltage across $\mathrm{L}_{\mathrm{LISN}}$ is u_L, across C_{LISN} is u_C, and the initial time is t_0, i_L, $i_{R,}$ and V_A can be solved as follows:

$$u_c(t) + R_{\mathrm{LISN}} i_R(t) = u_L(t) \tag{3}$$

$$u_c(t) = u_c(t_0) + \frac{1}{C_{\mathrm{LISN}}} \int_{t0}^{\tau=t} i_R(\tau)\, d\tau \tag{4}$$

$$u_L(t) = L_{\mathrm{LISN}} \frac{di_L}{dt} \tag{5}$$

$$i_L = i_{ac} - i_R. \tag{6}$$

Plugging (4)–(6) into (3) turns into (7)

$$\frac{d^2 i_R(t)}{dt^2} + \frac{R_{\mathrm{LISN}}}{L_{\mathrm{LISN}}} \frac{di_R(t)}{dt} + \frac{1}{L_{\mathrm{LISN}} C_{\mathrm{LISN}}} i_R(t) = \frac{d^2 i_{\mathrm{ac}}(t)}{dt^2}. \tag{7}$$

The curve of the current i_{ac} as a function of time is shown in Fig. 9, which is the very close to the measured one in Fig. 4 without background noise. The i_R can be calculated based on (7) and i_{ac}. The voltage spike on V_A can be calculated in (8) and is exactly the same as the simulated one in Fig. 9

$$V_A(t) = -\frac{1}{2} R_{\mathrm{LISN}} i_R(t). \tag{8}$$

The i_{ac} during the reverse recovery process is exclusively related to reverse recovery characteristics of diodes. The objective of this article is not to predict the reverse recovery currents of the diodes but to predict or model the measured EMI caused by the reverse recovery currents. It is therefore, reasonable and necessary to use the measured reverse recovery current i_{ac} to simulate the current distribution inside the LISNs (i_L and i_R) precisely. The measured current waveforms with the background noise removed in Fig. 4(b) is the current source we used for the simulation in Fig. 8. The simulated i_L , i_R, and V_A in MATLAB based on Fig. 8(b) and (3)–(8) as well as the measured i_{ac} are shown in Fig. 9. From Fig. 9, i_L and i_{ac} are almost identical except during t_3-t_4 short period when i_{ac} has an abrupt change. High *di/dt* of i_{ac} leads to part of i_{ac} flowing through R_{LISN} because of the high impedance of $\mathrm{L}_{\mathrm{LISN}}$ to the high *di/dt* current. i_R has a current spike due to the difference of i_L and i_{ac}. i_R flows through R_{LISN} and leads to a voltage spike on V_A. The -0.15 V voltage offset due to the 60 Hz leakage current flowing through R_{LISN} was also included in V_A's waveform. Comparing the curves in Fig. 9 with those in Fig. 4(b), they match very well. This proves that the voltage spike on V_A is due to the reverse recovery currents of the diode bridge.

In one ac line period, the voltage spike occurs twice in opposite directions. The other voltage spike can be calculated similarly. The calculated FFT of V_A in dBμV in one ac line period is plotted from 150 kHz to 30 MHz in Fig. 10. The magnitude of FFT spectrum is more than 30 dB lower than the measured EMI spectrum in Fig. 2. This phenomenon has been analyzed in [27] and will be explained in the following section.

III. Modeling of the Measured EMI

As shown in Figs. 2 and 10, the FFT spectrum is much lower (around 33dB) than the EMI measured with a spectrum analyzer. This is because the spectrum analyzers work in a different way from the FFT and this will be explained here.

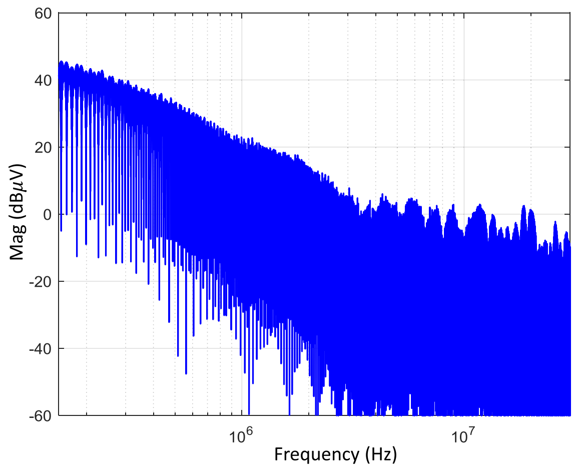

Fig. 10. FFT spectrum of the calculated V_A.

To analyze the measured DM EMI noise, the working principle of a spectrum analyzer should be considered in Fig. 11. The simulated waveforms V_A, which can be decomposed to a series of harmonics, in Fig. 9 is the input signal in Fig. 11. FFT calculates the magnitude of each order harmonic. On the other hand, based on the theory developed in [27] for spectrum analyzers, in Fig. 11, the spectrum analyzer first sweeps the frequencies by changing the frequency of the local oscillator. The mixer converts the harmonics at the swept frequencies to signals at a fixed intermediate frequency (IF). The converted harmonics, including those higher or lower than IF, are processed by an IF filter which has a -6 dB RBW. In EMI standard EN55022, the RBW is 9 kHz from 150 kHz to 30 MHz. Based on the theory in [27], when two or more orders of harmonics are located within 2RBW, these harmonics can stack up in the time domain at the output of the IF filter. The envelope detector catches the increased amplitude and feeds it to the peak, quasi-peak and average EMI detectors. The measured EMI noise could therefore be much higher than individual harmonics. The difference between peak detector and the other two detectors is the charging and discharging time constants, which are defined in EMI standards. For the voltage spikes in $\mathrm{V_A}$, the fundamental frequency of the spikes is 60 Hz, therefore, there are 300 orders of harmonics within 2RBW (18 kHz), so the measured EMI noise via a spectrum analyzer with 9 kHz RBW will be much higher than the FFT result.

To verify that the high peak EMI noise in Fig. 2 is caused by the voltage spikes resulted from the reverse recovery currents of the diode bridge, the FFT result in Fig. 10 was fed to the EMI prediction program developed in [27], which emulates the EMI measurement of an EMC spectrum analyzer. The predicted peak EMI is shown in Fig. 12 compared with the measured peak EMI and the EMI standard EN55022. The spectrum is very close to the measured EMI noise spectrum with very small difference in the range of 150 kHz–3 MHz. Above 3 MHz, the background EMI dominates in the measured EMI.

The predicted and the measured quasi-peak and average EMI are also compared in Fig. 13. They match very well. It is shown that the reverse recovery currents also increase the measured quasi-peak and average EMI. The quasi-peak EMI generated by the reverse recovery currents of the diodes is higher than the EMI standard.

The analysis above shows that, although the reverse recovery currents of the diodes repeat at a frequency of 50/60 Hz, they have a wide spectrum as shown in Fig. 10. Due to the operating principle of the EMC spectrum analyzers, the measured EMI spectrum is much higher than the calculated FFT spectrum of the 50/60 Hz reverse recovery currents. The measured spectrum can be higher than EMI standards as shown in Figs. 12 and 13. Because of this, the solutions must be proposed to reduce the EMI.

IV. EMI Noise Reduction Techniques

A. X-*Capacitor*

In Fig. 8(b), if an *X*-capacitor C_X across the two ac lines is added between the LISN and the diode rectifier as shown in Fig. 14(a), it can bypass the HF current flowing through R_{LISN}. An equivalent DM circuit used to analyze C_X is shown in Fig. 14(b).

The insertion gain IG of $\mathrm{C_X}$, which is defined as the ratio of u_R with C_X to that without C_X, is derived based on Fig. 14(b) and given by (9). For the peak EMI noise in Fig. 7, at 150 kHz, the EMI is 79 dBμV, which is 13 dB higher than the EMI standard 66 dBμV. C_X should achieve at least -13 dB insertion gain to meet the standard. Fig. 15 shows the insertion gain as a function of C_X at 150 kHz

$$\mathrm{IG} = \frac{s^2 L_{\mathrm{LISN}} C_{\mathrm{LISN}} + s C_{\mathrm{LISN}} R_{\mathrm{LISN}} + 1}{s^3 L_{\mathrm{LISN}} C_{\mathrm{LISN}} C_X R_{\mathrm{LISN}} + s^2 L_{\mathrm{LISN}} \left(C_{\mathrm{LISN}} + C_X\right) + s C_{\mathrm{LISN}} R_{\mathrm{LISN}} + 1}. \quad (9)$$

In Fig. 15, when $C_X > 70$ nF, the insertion gain will be more than -13 dB and EMI will meet the EMI standard. The positive insertion gain around C_X =10 nF in Fig. 15 is because of the pole due to C_X and L_{LISN}. To have more than 3 dB margin for EMI reduction, C_X is selected as 90 nF. Capacitor C_X should have good capacitive performance at 150 kHz. Fig. 16 shows the measured peak EMI at different C_X.

In Fig. 16, as predicted, 90 nF C_X can achieve around 5 dB margin. Fig. 17 shows the measured LISN's output voltage V_A. It is shown that as C_X increases, both the amplitude and slope (HF components) of V_A significantly reduces, as a result, the measured EMI is significantly reduced as in Fig. 16. Since LISNs are used to evaluate EMI only while there is no requirement for the stabilization time of V_A in EMI standard (EN55022), we optimize C_X based on the EMI attenuation requirement with the derived insertion gain in (9). The resonance frequency of V_A in Fig. 17 can be given by

$$f_r \approx \frac{1}{2\pi\sqrt{L_{\mathrm{LISN}}\left(C_{\mathrm{LISN}} + C_X\right)}}. \quad (10)$$

It should be pointed out that an ac line DM inductor cannot be used to reduce the EMI because the inductor results in a faster change of *di/dt* in the reverse recovery currents, which results in higher V_A and EMI.

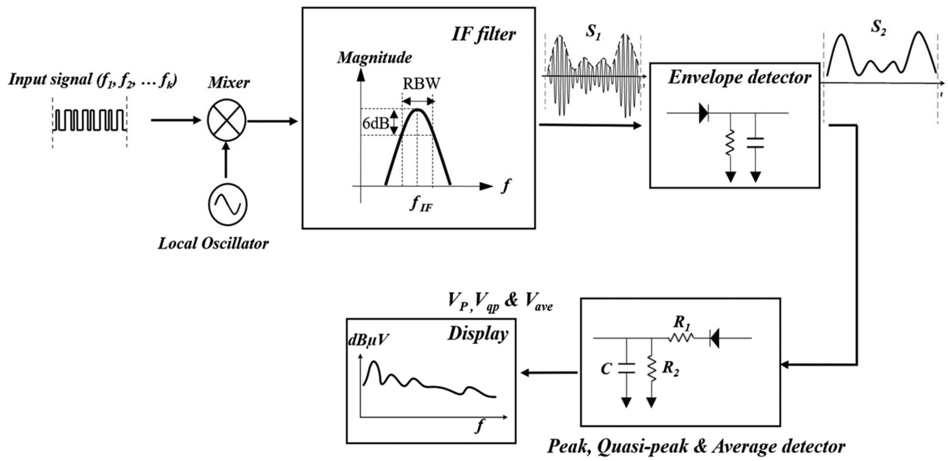

Fig. 11. Operating principle of a spectrum analyzer.

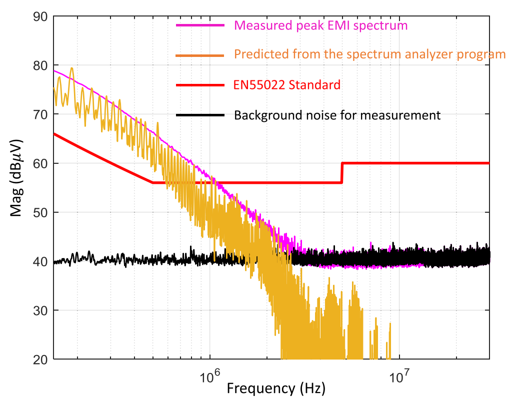

Fig. 12. Comparison of the measured and the predicted peak EMI due to the reverse recovery current of the diode bridge.

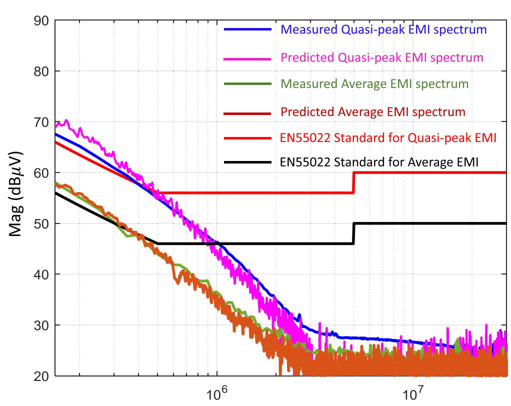

Fig. 13. Comparison of the measured and the predicted quasi peak and average EMI.

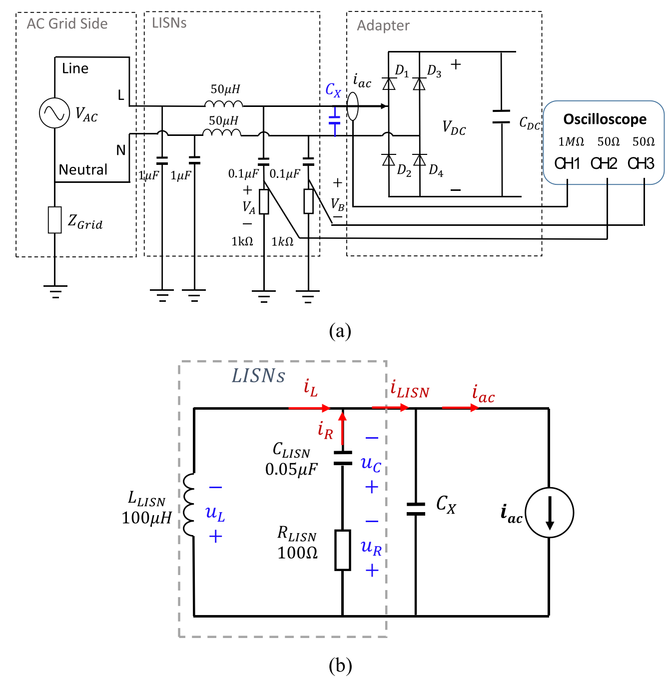

Fig. 14. (a) X-capacitor CX is added between the LISNs and the diode rectifier, (b) DM noise circuit model with an X-capacitor CX applied.

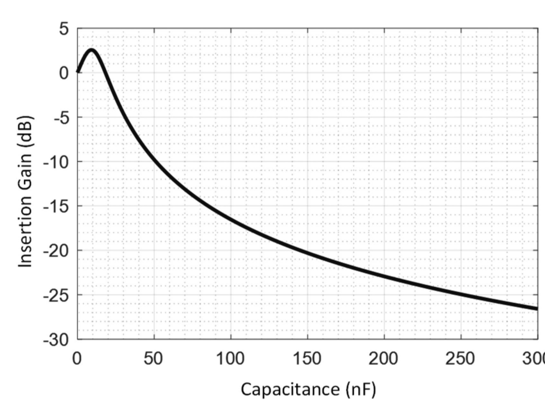

Fig. 15. Insertion gain of C_X.

The proposed EMI reduction techniques (X-capacitor) will not be influenced by the power level, as long as the impedance of X-capacitor is much smaller than the impedance of LISN's R-C (50 Ω-0.1μ F) branch to bypass most of the differential-mode (DM) EMI noise, which can be easily met within 150 kHz–30 MHz (conducted EMI frequency range specified by EN55022

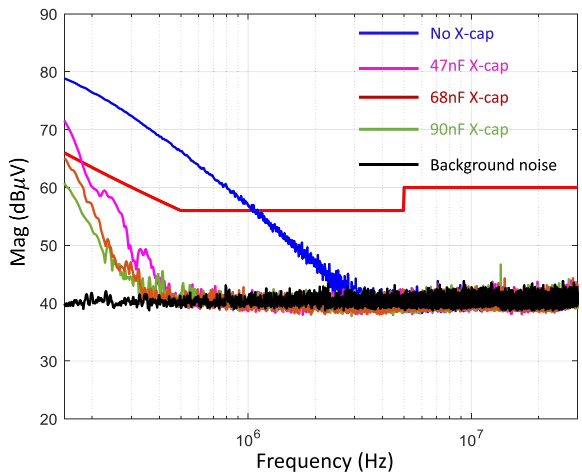

Fig. 16. Measured peak EMI with and without C_X.

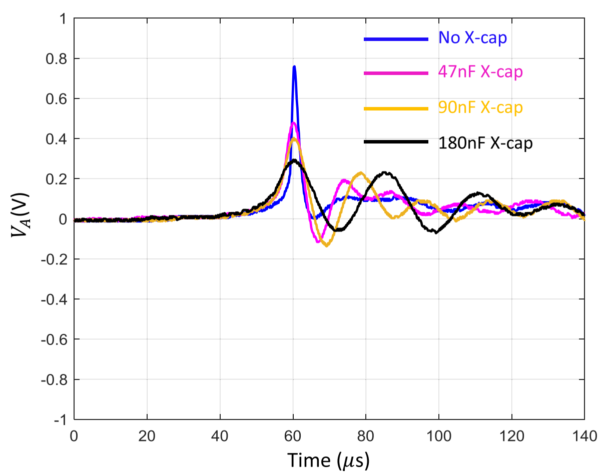

Fig. 17. Measured output voltage V_A on one LISN with different C_X.

standard). Typically, the bigger the power level, the bigger the forward current (i_{ac} during the diode bridge's on duration), and the bigger the reverse recovery charge, which leads to a bigger voltage spike on V_A. To reduce the EMI noise caused by the reverse recovery currents of diode rectifier at a higher power level to meet the EMI limit, a big capacitor may be needed. The capacitance needed for EMI reduction at 150 kHz can be calculated based on the derived insertion gain IG in (9), which also depends on how much EMI noise needs to be mitigated.

An *X*-capacitor has a big size, it introduces extra cost and may reduce the power factor of the converter, Therefore, an alternative technique is proposed below.

B. Fast Recovery Diodes

Because the voltage spikes are caused by the abrupt current slope change during the reverse recovery of the diode bridge as shown in Fig. 9, the EMI can be reduced using the diodes with fast and soft turn-OFF characteristics. In this article, the fast recovery diodes (MURC5J), ultrafast recovery diodes (STTH15RQ06) as well as Q-speed diodes (LXA08B600) are used to replace the original standard 50 /60 Hz diodes.

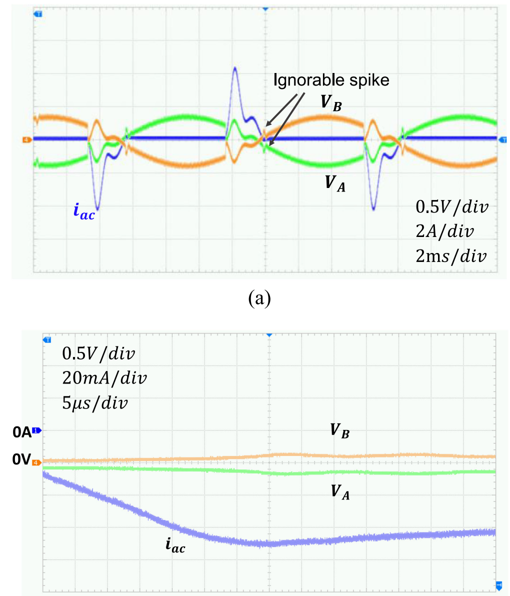

(a)

(b)

Fig. 18. (a) Fast-recovery diodes significantly reduce voltage spike on V_A. (b) Zoomed-in picture during the diode reverse recovery.

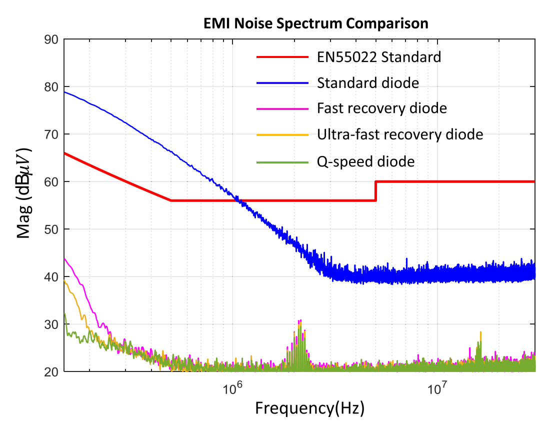

Fig. 19. Comparison of the measured EMI spectra with different types of diodes.

Fig. 18(a) and (b) shows the time domain waveforms on a LISNs' 50 Ω load resistance with the fast recovery diodes MURC5J (600 V/4 A, recovery time < 39 ns). Compared with that with original standard diodes (600 V/4 A, recovery time > 500 ns) in Fig. 4(a) and 4(b), it is shown that even without an *X*-capacitor, the fast recovery diodes can greatly reduce the voltage spike on V_A. As shown in Fig. 18, there is no abrupt current slope change during the reverse recovery. The time-domain waveforms for ultrafast recovery diodes STTH15RQ06 and Q-speed diodes LXA08B600 are similar to those of the fast recovery diodes in Fig. 18 so they are not shown here.

Fig. 19 compares the measured EMI spectra for four types of diodes tested in this article. It is found the Q-speed diodes have the lowest EMI and only the standard 50/60 Hz diodes violate the EMI standard. In Fig. 19, the standard diodes have a

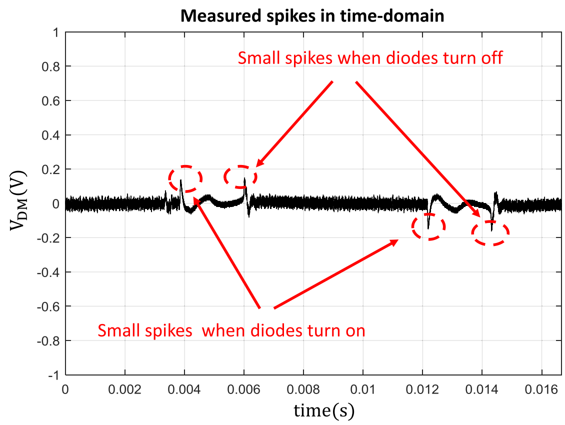

Fig. 20. Measured output voltage of the DM separator with fast diodes.

TABLE II
COST ESTIMATION (US DOLLAR) FOR *X*-CAPACITOR AND FAST RECOVERY DIODES TECHNIQUES

Solution 1	100nF C_X	Standard diodes	Overall	Cost/watt
Cost 1	\$0.10759	\$0.05805×4	\$0.3398	\$0.0052/W
Solution 2	No X cap	Fast recovery diodes	Overall	Cost/watt
Cost 2	\$0	\$0.18×4	\$0.72	\$0.0111/W

background EMI noise 20 dB higher than other diodes because a 20 dB attenuator was used in the measurement.

It should be pointed out that the current and voltage spikes during the $t_{\rm on}$ duration will not be changed, since it is determined by the input voltage and output power, which is unrelated to the reverse recovery characteristics of diodes. Also, it will not lead to EMI issues as discussed in Section II.

The advantage of replacing the standard diodes with fast recovery/ultrafast recovery/Q-speed diodes is that it will not increase the size of the power converter, which is usually preferred in high power density design.

Fig. 20 shows the measured waveform at the output of a DM separator. It is shown that, compared with that in Fig. 6, the second spike due to the reverse recovery of the diodes is significantly reduced. It results in a good EMI reduction in Fig. 19.

It should be pointed out that the fast recovery diode solution will also not be significantly influenced by the power level due to its internal soft turn-OFF characteristics. Typically, the higher the input voltage is, the higher the reverse voltage added across one pair of diodes is, and the smaller the reverse recovery time is, which leads to a higher voltage spike on V_A. However, since the spike are still very small, based on the experimental exploration, the technique is applicable from 100 to 240 V ac input voltage range (it is the whole input voltage range for power adapters) without problems.

C. Cost and Size Analysis

Table II gives the cost estimation for the proposed two techniques. The fast recovery diode solution will not increase the size of the power adapter; however, it is more expensive than the *X*-capacitor solution, so it is suitable for a high power density design rather than a low-cost design. On the other hand, the *X*-capacitor solution is cheaper than the fast recovery diode solution; however, the *X*-capacitor is bulky so it is suitable for a low-cost design rather than a high power density design (e.g., the size of a 100 nF *X*-capacitor: 18.00 × 6.00 × 11.10 mm).

V. CONCLUSION

In this article, the reverse recovery currents of 50/60 Hz diode bridges were identified as a major EMI noise source for ac/dc converters with dc-bus filters. The mechanism of how the diode reverse recovery currents generate EMI was disclosed and quantified. The EMI is predicted based on the operating principle of spectrum analyzers and it was found that the measured EMI can be much higher than the EMI standards. Two techniques were proposed to reduce the EMI due to the reverse recovery of the diode bridge. The theoretical analysis was validated by both simulations and experiments.

The contributions of this article are as follows.

1) The mechanism of EMI generated from the reverse recovery currents of 50/60 Hz diode bridges is disclosed and the effect of the reverse recovery currents on the EMI is quantified.
2) An *X*-capacitor solution is proposed, and the insertion gain is derived for quantified analysis. Based on that, designers no longer need to use the trial-and-error method to find the capacitance for EMI reduction.
3) Fast recovery diodes, ultrafast recovery diodes, or Q-speed diodes can be used as the diode bridge to reduce the EMI.

REFERENCES

[1] Y. Li, L. Yang, S. Wang, H. Sheng, S. Lakshmikanthan, and L. Jia, “Investigation of a DC bus differential mode EMI filter for AC/DC power adapters,” in *Proc. IEEE Appl. Power Electron. Conf. Expo.*, 2018, pp. 603–610.
[2] Y. Li, S. Wang, H. Sheng, and S. Lakshmikanthan, “Investigate and reduce capacitive couplings in a flyback adapter with a DC-bus filter to reduce EMI,” *IEEE Trans. Power Electron.*, vol. 35, no. 7, pp. 6963–6973, Jul. 2020.
[3] S. Wang, F. C. Lee, and W. G. Odendaal, “Characterization, evaluation, and design of noise separator for conducted EMI noise diagnosis,” *IEEE Trans. Power Electron.*, vol. 20, no. 4, pp. 974–982, Jul. 2005.
[4] F. C. Lee, M. Xu, S. Wang, and B. Lu, “Design challenges for distributed power systems,” in *Proc. CES/IEEE Int. Power Electron. Motion Control Conf.*, 2006, pp. 1–15.
[5] B. Zhang and S. Wang, “A survey of EMI research in power electronics systems with wide-bandgap semiconductor devices,” *IEEE J. Emerg. Sel. Topics Power Electron.*, vol. 8, no. 1, pp. 626–643, Mar. 2020.
[6] S. Wang, F. C. Lee, and W. G. Odendaal, “Single layer iron powder core inductor model and its effect on boost PFC EMI noise,” in *Proc. IEEE Annu. Conf. Power Electron. Specialist*, 2003, pp. 847–852.
[7] F. Luo, D. Dong, D. Boroyevich, P. Mattavelli, and S. Wang, “Improving high-frequency performance of an input common mode EMI filter using an impedance-mismatching filter,” *IEEE Trans. Power Electron.*, vol. 29, no. 10, pp. 5111–5115, Oct. 2014.
[8] S. Wang, F. C. Lee, D. Y. Chen, and W. G. Odendaal, “Effects of parasitic parameters on EMI filter performance,” *IEEE Trans. Power Electron.*, vol. 19, no. 3, pp. 869–877, May 2004.
[9] J. Yao, Y. Li, Z. Ma, and S. Wang, “Advances of modeling and reduction of conducted and radiated EMI in flyback converters,” in *Proc. IEEE Energy Convers. Congr. Expo.*, 2020, pp. 3362–3369.
[10] J. Yao, Y. Li, S. Wang, X. Huang, and X. Lyu, “Modeling and reduction of radiated EMI in a GaN IC-based active clamp flyback adapter,” *IEEE Trans. Power Electron.*, vol. 36, no. 5, pp. 5440–5449, May 2021.
[11] J. Yao, Y. Lai, Z. Ma, and S. Wang, “Advances in modeling and reduction of conducted and radiated EMI in non-isolated power converters,” in *Proc. IEEE Appl. Power Electron. Conf. Expo.*, 2021, pp. 2305–2312.

[12] P. Kong and F. C. Lee, "Transformer structure and its effects on common mode EMI noise in isolated power converters," in *Proc. IEEE Appl. Power Electron. Conf. Expo.*, 2010, pp. 1424–1429.
[13] P. Kong, S. Wang, and F. C. Lee, "Reducing common mode EMI noise in two-switch forward converter," in *Proc. IEEE Energy Convers. Congr. Expo.*, 2009, pp. 3622–3629.
[14] H. Zhang, S. Wang, Y. Li, Q. Wang, and D. Fu, "Two-capacitor transformer winding capacitance models for common-mode EMI noise analysis in isolated DC–DC converters," *IEEE Trans. Power Electron.*, vol. 32, no. 11, pp. 8458–8469, Nov. 2017.
[15] Y. Li, H. Zhang, S. Wang, H. Sheng, C. P. Chng, and S. Lakshmikanthan, "Investigating switching transformers for common mode EMI reduction to remove common mode EMI filters and Y-capacitors in flyback converters," *IEEE J. Emerg. Sel. Topics Power Electron.*, vol. 6, no. 4, pp. 2287–2301, Dec. 2018.
[16] D. Jiang, R. Lai, F. Wang, F. Luo, S. Wang, and D. Boroyevich, "Study of conducted EMI reduction for three-phase active front-end rectifier," *IEEE Trans. Power Electron.*, vol. 26, no. 12, pp. 3823–3831, Dec. 2011.
[17] Z. Ma, Y. Li, S. Wang, H. Sheng, S. Lakshmikanthan, and D. Osterhout, "Investigation and reduction of a low-frequency EMI noise of AC/DC power adapters with diode bridge as input rectifier," in *Proc. IEEE Int. Power Electron. Motion Control Conf. Expo* ., 2020, pp. 3085–3091.
[18] R. Scheich and J. Roudet, "EMI conducted emission in the differential mode emanating from an SCR: Phenomena and noise level prediction," *IEEE Trans. Power Electron.*,vol. 10, no. 2, pp. 105–110, Mar. 1995.
[19] H. Rathnayake, F. Zare, D. Kumar, A. Ganjavi, and P. Davari, "Nonlinear effects of three-phase diode rectifier on noise emission in the frequency range of 2–9 kHz," in *Proc. IEEE Int. Conf. Power Electron., Drives Energy Syst.*, 2020, pp. 1–6.
[20] J. E. Makaran, "MOSFET gate charge control through observation of diode forward and reverse recovery behaviour," in *Proc. IEEE Elect. Power Energy Conf.*, 2015, pp. 478–483.
[21] X. Yuan, S. Walder, and N. Oswald, "EMI generation characteristics of SiC and Si diodes: Influence of reverse-recovery characteristics," *IEEE Trans. Power Electron.*,vol. 30, no. 3, pp. 1131–1136, Mar. 2015.
[22] S. Tiwari, S. Basu, T. M. Undeland, and O. Midtgård, "Efficiency and conducted EMI evaluation of a single-phase power factor correction boost converter using state-of-the-art SiC MOSFET and SiC diode," *IEEE Trans. Ind. Appl.*, vol. 55, no. 6, pp. 7745–7756, Nov./Dec. 2019.
[23] Y. Liu, S. Cordes, T. Geinzer, J. Thiele, M. Thoben, and A. Lindemann, "Comparison of EMI behavior in inverter and buck-converter operation of power modules by considering the diode reverse recovery effects," in *Proc. CIPS Int. Conf. Integr. Power Electron. Syst.*, 2016, pp. 1–6.
[24] T. Ibuchi and T. Funaki, "Effect of diode characteristics on conducted noise spectrum in CCM boost converter," in *Proc. IEEE Int. Symp. Electromagn. Compat.*, 2014, pp. 59–64.
[25] R. W. Erickson and D. Maksimovic, *Fundamentals of Power Electronics*, 2nd ed., Norwell, MA, USA: Klewer, 2001.
[26] C. L. Ma and P. O. Lauritzen, "A simple power diode model with forward and reverse recovery," *IEEE Trans. Power Electron.*, vol. 8, no. 4, pp. 342–346, Oct. 1993.
[27] L. Yang, S. Wang, H. Zhao, and Y. Zhi, "Prediction and analysis of EMI spectrum based on the operating principle of EMC spectrum analyzers," *IEEE Trans. Power Electron.*, vol. 35, no. 1, pp. 263–275, Jan. 2020.

Zhedong Ma (Student Member, IEEE) received the B.Eng. degree in electrical engineering and automation from Zhejiang University, Hangzhou, China, in 2019. He is currently working toward the Ph.D. degree in power electronics with the University of Florida, Gainesville, FL, USA.

He has authored and coauthored more than ten IEEE journal and conference papers since 2019. His research interests include electromagnetic interference/compatibility (EMI/EMC) in power electronics systems, magnetic components, and wireless charging.

Yiming Li received the B.S.E.E. degree from Zhejiang University, Zhejiang, China, in 2015, and the Ph.D. degree from the University of Florida, Gainesville, FL, USA, in 2019, both in electrical engineering.

In 2020, he was a Senior Application Engineer with Monolithic Power Systems. He is also studying on transformer and electromagnetic interference filter design and optimization for switching mode power supplies. He has authored and coauthored more than 20 IEEE journal and conference papers since 2017. His research interests include electromagnetic interference and compatibility in power electronic systems.

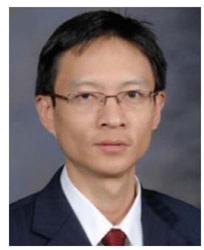

Shuo Wang (Fellow, IEEE) received the Ph.D. degree in electrical engineering from Virginia Tech, Blacksburg, VA, USA, in 2005.

He is currently a Full Professor with the Department of Electrical and Computer Engineering, University of Florida, Gainesville, FL, USA. He has authored or coauthored more than 200 IEEE journal and conference papers and holds around 30 pending/issued U.S./international patents.

Dr. Wang was the recipient of the Best Transaction Paper Award from the IEEE Power Electronics Society in 2006 and two William M. Portnoy Awards for the papers published in the IEEE Industry Applications Society in 2004 and 2012, and the Distinguished Paper Award from the 2022 IEEE Symposium on Security and Privacy. In 2012, he was also the recipient of the prestigious National Science Foundation CAREER Award. He is currently an Associate Editor for the IEEE TRANSACTIONS ON INDUSTRY APPLICATIONS and the IEEE TRANSACTIONS ON ELECTROMAGNETIC COMPATIBILITY. He is the Chair of Power Electronics EMI/EMC Special Committee of IEEE EMC Society and an Instructor of IEEE Clayton Paul Global University. He was a Technical Program Co-Chair of the IEEE 2014 International Electric Vehicle Conference.

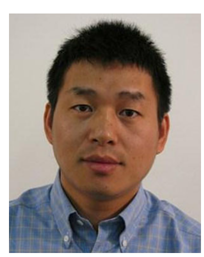

Honggang Sheng received the B.S. degree from Xi'an Jiaotong University, Xi'an, China, in 1998, the M.S. degree from the South China University of Technology, Guangzhou, China, in 2003, and the Ph.D. degree from Virginia Polytechnic Institute and State University, Blacksburg, VA, USA, in 2009, all in electrical engineering.

Since 2011, he has been with Google, Inc., Mountain View, CA, USA, as a Power Engineer for the data center and consumer hardware.

Srikanth Lakshmikanthan has been the Technical Power Team Manager with Google Hardware, Mountain View, CA, USA, since 2016. He has been a Staff Hardware Engineer with Google, Mountain View, and led power design solutions in multiple product areas, including data center and Chrome Hardware, since 2006.